JOURNAL OF CATALYSIS 157, 423–435 (1995)

Isomerization of *n*-Butene to Isobutene by Ferrierite and Modified Ferrierite Catalysts

R. J. Pellet, D. G. Casey, H.-M. Huang, R. V. Kessler, E. J. Kuhlman, C.-L. O'Young, R. A. Sawicki, and J. R. Ugolini

Texaco Group Inc., P.O. Box 509, Beacon, New York 12508

Received February 15, 1995; revised July 12, 1995; accepted August 4, 1995

n-Butene was isomerized to isobutene over fresh and used ferrierite catalysts. Activity and selectivity for skeletal isomerization and biproduct formation were measured and changes following extended use were related to changes in ferrierite's aluminum distribution. In its fresh form, ferrierite exhibited high activity for *n*-butene conversion and high selectivity for non-C_4 products with reduced selectivity for isobutene. With time on feed, side-product formation decreased and isobutene yields reached a maximum, then declined with further time on feed. After several run/regeneration cycles, a marked drop-off in the maximum achievable isobutene yield was observed and selectivity for non-C_4 products increased. MAS-NMR of the deactivated catalyst showed a decrease in zeolitic, tetrahedral aluminum and an increase in octahedral aluminum. In order to understand changes occurring following extended use, ferrierite powders were modified by steam and by steam plus acid-wash treatments. A steamed ferrierite catalyst exhibited lower initial *n*-butene conversion; however, selectivity to non-C_4 products increased relative to that of the fresh catalyst. XRD peak areas and gravimetric adsorption data indicated excellent crystallinity retention following steam treatment; XRD unit cell determination, and FTIR and NMR analysis suggested significant framework dealumination and the creation of a nonframework aluminum phase. TEM suggested that at least a portion of this phase exists in mesopores created by steam treatment. A steamed–acid-washed ferrierite catalyst also exhibited reduced initial *n*-butene conversion but high isobutene selectivity throughout the run. Biproduct formation was greatly reduced. Characterization indicated that acid-wash treatment after steaming had no effect on framework aluminum but partially reduced the amount of nonframework aluminum. Steamed–acid-washed ferrierite was much less sensitive to subsequent hydrothermal treatments than was the starting ferrierite. The study suggests a catalytic role for nonframework alumina, generated upon extended use of unmodified ferrierite and present in steamed ferrierite. Catalytically active, nonframework sites contribute to the production of non-C_4 products and reduced isobutene selectivity. Steamed–acid-washed ferrierite with the active nonframework phase removed exhibits excellent isobutene selectivity and catalytic stability.

INTRODUCTION

Government legislation and environmental concerns continue to change the compositional makeup of gasoline. Current legislation has mandated the addition of oxygenates to the gasoline pool in certain areas in order to reduce carbon monoxide formation. MTBE (methyl *t*-butyl ether) is the most widely used oxygenate for this purpose although other oxygenates can contribute (1). As its use increases, production (from methanol and isobutene) may become limited by the availability of isobutene, currently supplied by the catalytic cracking of petroleum. Skeletal isomerization of linear butenes to isobutene represents a potential route to supplement current sources.

The skeletal isomerization of olefins over acid catalysts has been reviewed (2). Much of the early work employed amorphous acids such as halogenated aluminas but more recently, a number of papers and patents describe (3–8) the use of zeolites and particularly 10-member (10-MR) ring zeolites for skeletal isomerization because of their enhanced ability to resist coking and inhibit the production of unwanted side products by shape selectivity. Of all the zeolites evaluated, ferrierite is reported to exhibit the highest selectivity for isobutene (9, 10). Its improved selectivity has been related to its pore structure.

Ferrierite has an orthorhombic framework containing one-dimensional channels of 10-member rings (4.2 × 5.4 Å) and one-dimensional channels of 8-member rings (8-MR) (3.5 × 4.8 Å). These two kinds of channels are perpendicularly intersected (11). High isomerization selectivity has been attributed to spatial constraints at the intersection of the 8-MR and 10-MR channel systems which restrict bimolecular reaction intermediates involved in side-product formation (10). Alternatively, ferrierite's selectivity has been attributed to its channel dimensions. Modeling studies reveal that ferrierite offers the highest diffusion barrier for trimethylpentene migration and might be expected to best resist the escape of branched C_8 isomers from the zeolite crystal; it has been proposed that C_8

0021-9517/95 $12.00

olefins are intermediates in isobutene and side-product formation (9).

Ferrierite's selectivity in butene isomerization is affected by coke formation (12). During isomerization, channels of ferrierite are blocked by carbonaceous deposits formed early in the run. Improved selectivity for isobutylene and the repression of dimerization with time on stream were attributed to coke poisoning of strong acid sites or alternatively to increased spatial restrictions limiting bimolecular reactions.

Because deactivation is observed (12), it is likely that any commercial process using ferrierite for butene isomerization must include an oxidative regeneration step in order to remove coke deposits responsible for deactivation. By its nature, oxidative regeneration will subject the ferrierite catalyst to hydrothermal treatment. Hydrothermal treatment of ferrierites leads to formation of nonframework aluminum (13, 14). Interestingly, acid treatment of steamed ferrierites is only partially successful in removing this nonframework aluminum. Steamed and acid-washed ferrierites exhibited a decrease in catalytic activity for such reactions as alkane cracking and methanol conversion (13).

In this study, the catalytic behavior of modified ferrierites has been investigated in order to better understand factors that affect performance before and after regeneration. The effect of steam and steam–acid-wash treatments on butene isomerization activity and selectivity are explored. Changes in ferrierite's physical characterization caused by hydrothermal treatment are measured and related to changes observed in performance. The significance of nonframework zeolitic alumina is inferred from the effect of acid-wash treatment on performance.

EXPERIMENTAL

Materials. Two ferrierite samples (provided by Tosoh USA, Inc. of Atlanta, Georgia) were used for all characterization, modifications, and catalyst performance evaluations reported herein. An alumina-bound ferrierite extrudate, commercially available as TSZ-720, contained 80% ferrierite and 20% alumina binder. This material was ammonium exchanged in aqueous solution to give a final potassium content of 0.19% and a sodium content below 0.05%. The ammonium-exchanged ferrierite was then calcined at 873°K in air for 4 h to generate hydrogen ferrierite extrudates, designated H-FER-1. Following ammonium exchange the chemical composition of the extrudate was 31.27% Si, 13.6% Al, 0.19% K, and less than 0.05% Na.

A ferrierite powder, commercially available as HSZ-720KOA, was analyzed to contain 39.5% Si, 4.32% Al, 1.11% Na, and 4.7% K. This material was also ammonium exchanged to achieve a potassium content of 0.22% and a sodium content of less than 0.05%. This powder was calcined as above to prepare the hydrogen ferrierite powder designated H-FER-2.

Ferrierite modifications. A steamed ferrierite sample, designated S-FER-2, was prepared from ammonium ferrierite powder by heating in a 100% flowing steam atmosphere at 873°K for 1 h. A steamed then acid-washed sample, designated SAW-FER-2, was prepared by slurrying the S-FER-2 powder in 5% hydrochloric acid solution at 350°K for 1 h, then washing in excess water to remove chloride; this wash treatment was repeated two additional times before finally drying and calcining in flowing air at 870°K. A steamed–acid-washed then steamed sample, designated SAWS-FER-2, was prepared from SAW-FER-2 using the same steam procedure described for S-FER-2.

Catalyst preparation. In order to evaluate the catalytic properties of the fresh and modified ferrierites described above, all powders were first formed into pellets by mixing with alumina binder, Dispal (manufactured and sold by Vista Chemical Co. of Houston, TX) in a physical mixer with added water to form a paste suitable for extrusion. The mixture was extruded to $\frac{1}{16}$", dried at 390°K overnight in air, and then calcined at 873°K for 2 h in a flowing air atmosphere. Catalysts prepared from H-FER-2, S-FER-2, SAW-FER-2, and SAWS-FER-2 were all prepared to contain 40% binder. Prior to bench scale evaluation, all calcined catalysts were ground and sieved to obtain a 20/40 U.S. Sieve Series mesh size fraction.

Bench scale catalyst evaluation. Butene isomerization reactions were carried out in a microreactor loaded with 1.0 g of meshed catalyst at 14.7 psia (1.0133×10^5 Pa). The reactor was heated from room temperature to 823°K at a ramping rate of 15°K/min in a flow of nitrogen of 60 ml/min. The temperature of the reactor was maintained at 823°K for 30 min. The reactor was cooled to 693°K and the nitrogen flow was switched to a mixture of 1-butene and nitrogen (1 : 1 molar ratio). The flow rate of butene was controlled to 5.3 g per hour. Reaction products were analyzed every hour with an on-line Hewlett–Packard 5890 Series II GC equipped with a capillary column capable of separating all components of significance. Butene conversion is defined as the weight percent change in linear butene content (1-, *cis,* and *trans*) in the feed and product mixture. A rate of conversion can be calculated as the number of moles of linear butenes converted per hour per gram of catalyst. Since all runs employed the same feed rate of 5.3 g of 1-butene per gram of catalyst per hour, 100% conversion would correspond to 0.57 mol/h-g catalyst. Yield_i is defined as the weight percent of a product$_i$ per weight of 1-butene feed (i.e., weight percent on feed).

Pilot plant catalyst evaluation. Catalyst H-FER-1 was evaluated at the pilot plant scale (400 cc catalyst load)

using actual C4 raffinate feed obtained following MTBE processing. The catalyst was tested for 26 cycles lasting 24 h each at temperatures ranging from 623 to 753°K, pressures from 20 to 45 psia (1.37×10^5 to 3.10×10^5 Pa) and at feed rates ranging from 0.8 to 3.2 WHSV. Following each test cycle, the catalyst was oxidatively regenerated *in situ* using nitrogen-reduced air to obtain controlled coke burns at temperatures ranging from 693 to 833°K. Following the last regeneration, the catalyst was discharged and analyzed to contain less than 0.4% coke. This used catalyst is designated as used-FER-1. Details of pilot plant evaluation will be reported elsewhere.

Sorption experiments. Sorption experiments were performed on a Kahn microbalance. Samples were first outgassed at 625°K overnight and then exposed to adsorbates at $P/P_0 = 0.1$ pressure. Adsorbates used for this study were *n*-pentane and carbon dioxide.

Infrared studies. Fourier transform infrared (FTIR) spectroscopy experiments were done on a Bio-Rad FTS-40 spectrometer at a resolution of 4 cm^{-1} using a diffuse reflectance accessory. The samples were ground into a fine powder using a mortar and pestle, and were then cut back to approximately 5% in ground KBr.

X-ray diffractions. Powder X-ray diffraction (XRD) scans were obtained using a Scintag PAD V diffractometer with a copper target X-ray source and a high purity germanium solid state detector to resolve the Cu$K\alpha$ radiation. Beam collimation was accomplished using a 2° divergence slit and a 0.3-mm receiving slit. Data were collected in 0.02° steps in the range $2° < 2\theta < 70°$. For determination of unit cell parameters, peak positions of eight selected *hkl*'s (200, 020, 101, 011, 411, 002, 510, and 202) were corrected using silicon as an internal standard. Results were calculated based on orthorhombic cell geometry using Scintag's lattice refinement software.

Aluminum MAS-NMR. The solid-state ^{27}Al NMR spectra were acquired at 78.3 MHz on a Varian Unity-300 wide bore spectrometer equipped with a 7-mm Chemagnetics CPMAS probe. The reference standard was KAl $(SO_4)_2 \cdot 10H_2O$ (0 ppm). Magic angle spinning (MAS) was utilized with typical spinning rates of 6–7 kHz. In order to selectively observe the central $\pm\frac{1}{2}$ quadrupolar transition, one can employ the selective solid-echo sequence (15–17): $(90°)_s$—τ—$(180°)_s$—τ—acquire. In this sequence the selective 90° pulsewidth is determined by dividing the nonselective 90° pulse (obtained from an aqueous solution of $KAl(SO_4)_2$) by a factor of $(I + \frac{1}{2})$, where I for ^{27}Al is $\frac{5}{2}$. Thus, the nonselective pulse was found to be 5 μs, and the selective pulse width that was employed was 1.7 μs; echo delays (τ) of 145 μs were employed. The echo delays were the inverse of the MAS spinning speed. In order to accentuate the differences between samples we have utilized the differing relative responses of aluminum sites with large and small quadrupole coupling constants to the nonselective solid-echo sequence, in which selective (1.7 μs) pulses are replaced by nonselective (5 μs) pulses. Use of a nonselective pulse in this manner serves to accentuate the signal observed from high symmetry sites (small quadrupole coupling constant). This is particularly useful in accentuating the signal from high symmetry tetrahedral framework aluminum, and octahedral extra-framework aluminum, with respect to lower symmetry extra-framework aluminum. This allows a partial spectral editing of the spectra so that signals arising from the binder alumina material are reduced and differences in zeolite structure can be observed more clearly. We have also obtained semi-quantitative ^{27}Al NMR spectra by a simple pulse-and-acquire sequence in which a small tip angle of 6° is used. Recycle delays of 0.2 s were used along with 5 ms acquisition times.

Modeling. Sorption at a fixed loading of one molecule was used to study relative adsorption energy, siting, and possible migration paths for the Al(O)OH and $Al(OH)_3$ at 873°K. Sorption studies at fixed pressure were carried out under experimental conditions for pentane and CO_2 to help understand experimental sorption results. The ferrierite model consisted of silicon and oxygen atoms with a cell size of 1 by 2 by 3 unit cells. In all calculations the ferrierite atom locations were fixed. Cerius (18) was used for all modeling. The Burchart/Universal force field (19, 20), available in Cerius, was used. Burchart charges were used for the ferrierite; charges for the aluminum compounds were calculated by charge equilibration (21). In the sorption runs Ewald summation with a cutoff of 9.5 Å was used for coulomb energy calculation.

X-ray photoelectron spectroscopy. XPS analysis was performed on a VG Instruments ESCALAB 5, Mk1 system. XPS data were collected with Mg$K\alpha$ X rays at 300 W. Samples were prepared for XPS analysis by mounting on powder sample stubs as a parallel array with silver paint. The samples were oriented parallel to the X-ray beam in order to eliminate beam shadowing. Photoelectron binding energies were referenced to adventitious carbon at 284.7 eV. Relative areas for the Al 2*p* and the Si 2*p* photoelectron peaks were calculated after linear background subtraction. VG-supplied sensitivity factors were used to calculate atomic fractions.

Transmission electron microscopy. Zeolite crystal changes following steam treatment were studied using a Philips TEM 420 electron microscope using a 120-KeV electron beam. Steamed zeolite crystals were first embedded in araldite epoxy and thin slices (approximately 60 nm thick) of the embedded sample were prepared by microtoming using a diamond knife. The slices were captured on Cu TEM grids and carbon coated prior to inspection.

RESULTS AND DISCUSSION

Unmodified ferrierite characterization and performance. Alumina-bound hydrogen ferrierite has been evaluated for butene isomerization activity and selectivity at the bench and pilot scale. A description of the pilot plant study is provided under Experimental; details will be presented elsewhere. Typical results obtained in bench scale isomerization of 1-butene with catalyst H-FER-1 are presented in Fig. 1. From the figure it can be seen that initial ferrierite conversion as measured by the disappearance of linear butenes is quite high (about 70%). This conversion is due in part to isomerization to isobutene (about 25%) but to a greater extent due to the formation of non-C_4 products, consisting largely of C_3 and C_5 olefins (over 40% conversion). The C_4 olefin distribution is close to that predicted by thermodynamic equilibrium (22). Formation of side products has been attributed to dimerization of *n*-butene feed or isobutene primary product to form octene intermediates; these intermediates are then cracked to yield the secondary non-C_4 olefinic products (9, 10). With time on feed, H-FER-1 loses its high initial activity; all of this loss is due to a decrease in the nonselective reactions. The C_4 olefin distribution remains relatively constant during this stage of reaction and near equilibrium, and conversion to isobutene actually increases. The improvement in isobutene selectivity with time on feed has been observed elsewhere and attributed to blocking or modification of nonselective sites by coke deposition (12). At about 20 h on feed, isobutene yield reaches a maximum, which thereafter declines. In the latter portions of the run, nonselective reactions are minimal and isobutene selectivity is very high, approaching 95%. Similar results were obtained in pilot plant tests, which also showed that initial high activity could be largely restored by oxidative regeneration supporting coke involvement in the initial activity attenuation.

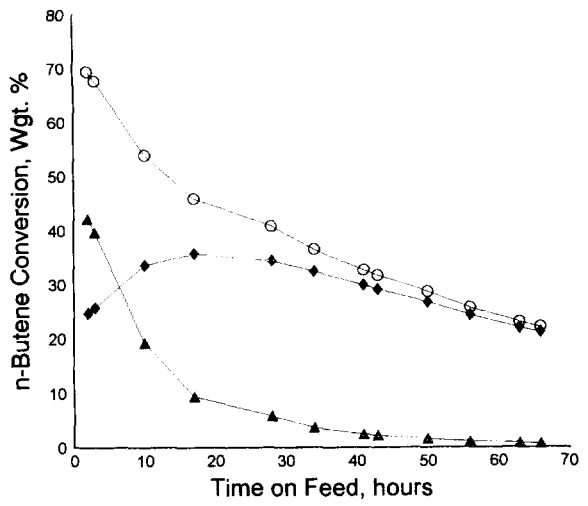

FIG. 1. Unmodified ferrierite catalyzed conversion of linear butenes: total conversion (circles), conversion to isobutene (diamonds), and to non-C_4 products (triangles).

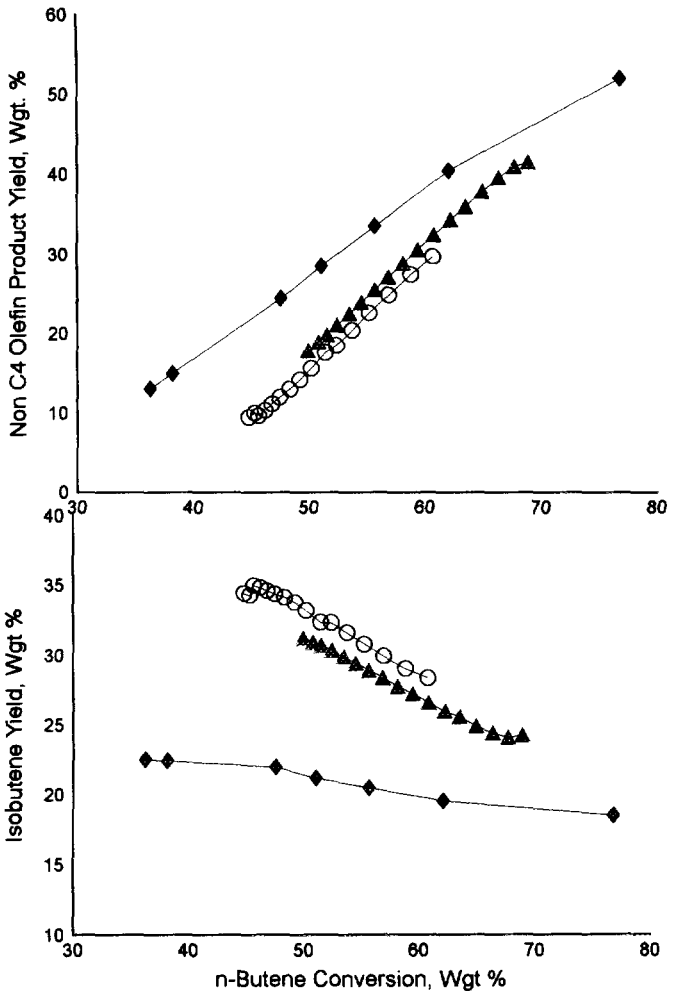

FIG. 2. Ferrierite selectivity before (circles) and after extended pilot plant evaluation (diamonds) and after acid-wash treatment (triangles) of the used catalyst.

In an effort to assess longer term trends and optimize processing conditions, H–FER-1 was evaluated for butene isomerization over 26 deactivation/regenerations cycles in the pilot reactor. Following a final oxidative regeneration, a portion of this used catalyst, used-FER-1, was recovered, analyzed to contain less than 0.4% carbon and then evaluated at the bench scale as described above. An additional portion of used-FER-1 was acid washed and also tested in the bench scale reactor. Results of these evaluations are presented in Fig. 2. Here product yields are plotted against linear butene conversions in order to allow comparisons to be made between catalysts at similar conversion levels. From Fig. 2, it can be seen that the used catalyst has increased selectivity for the production of non-C_4 products

and reduced selectivity toward isobutene. For example at 50% conversion, the fresh H-FER-1 yielded about 15% non-C_4 products and about 35% isobutene. By comparison, the used catalyst yielded about 28% non-C_4's and only 22% isobutene. Following acid-wash treatment, the used catalyst performance was almost entirely restored, yielding about 18% non C_4's and 32% isobutene.

Figure 3 presents ^{27}Al nonselective-echo MAS spectra of (a) fresh and (b) used ferrierite catalysts containing binder. Both spectra are plotted on the same vertical scale. The fresh catalyst shows a strong signal at about 58 ppm, indicative of aluminum in a tetrahedral environment, as expected for aluminum contained in the ferrierite crystal framework. In addition, a resonance at 0 ppm is observed, which can be attributed to aluminum in an octahedral environment. This signal at 0 ppm is due largely to the alumina binder used in catalyst preparation. While NMR does not allow us to quantify the relative amounts of aluminum in each form for each catalyst, comparisons between fresh and used catalyst spectra indicate a significant decrease in the relative amount of framework tetrahedral alumina for the used catalyst when compared to the fresh catalyst. This suggests that following multiple use and oxidative regeneration cycles, there is significant framework dealumination and the creation of a nonframework alumina phase in the used sample. The dealumination is most probably caused by the hydrothermal steaming conditions created by the oxidative coke burn step. The reason for the difference in signal-to-noise ratio is probably due to the loss of much of the aluminum NMR signal for the regenerated catalyst during the dead time of the echo experiment. As the sample becomes dealuminated the aluminum assumes a variety of distorted symmetries which have large quadrupole interactions. These large quadrupole interactions are directly related to short T2 relaxation times for these aluminum sites. In the 260-μs dead time of the echo delays the signal from these distorted aluminums is lost. Thus, in the regenerated sample, as framework aluminum is lost from the ferrierite framework, it assumes a lower symmetry and is lost from the spectrum, yielding a lower signal-to-noise spectrum than the fresh catalyst. The nonselective-echo experiment was used here to re-

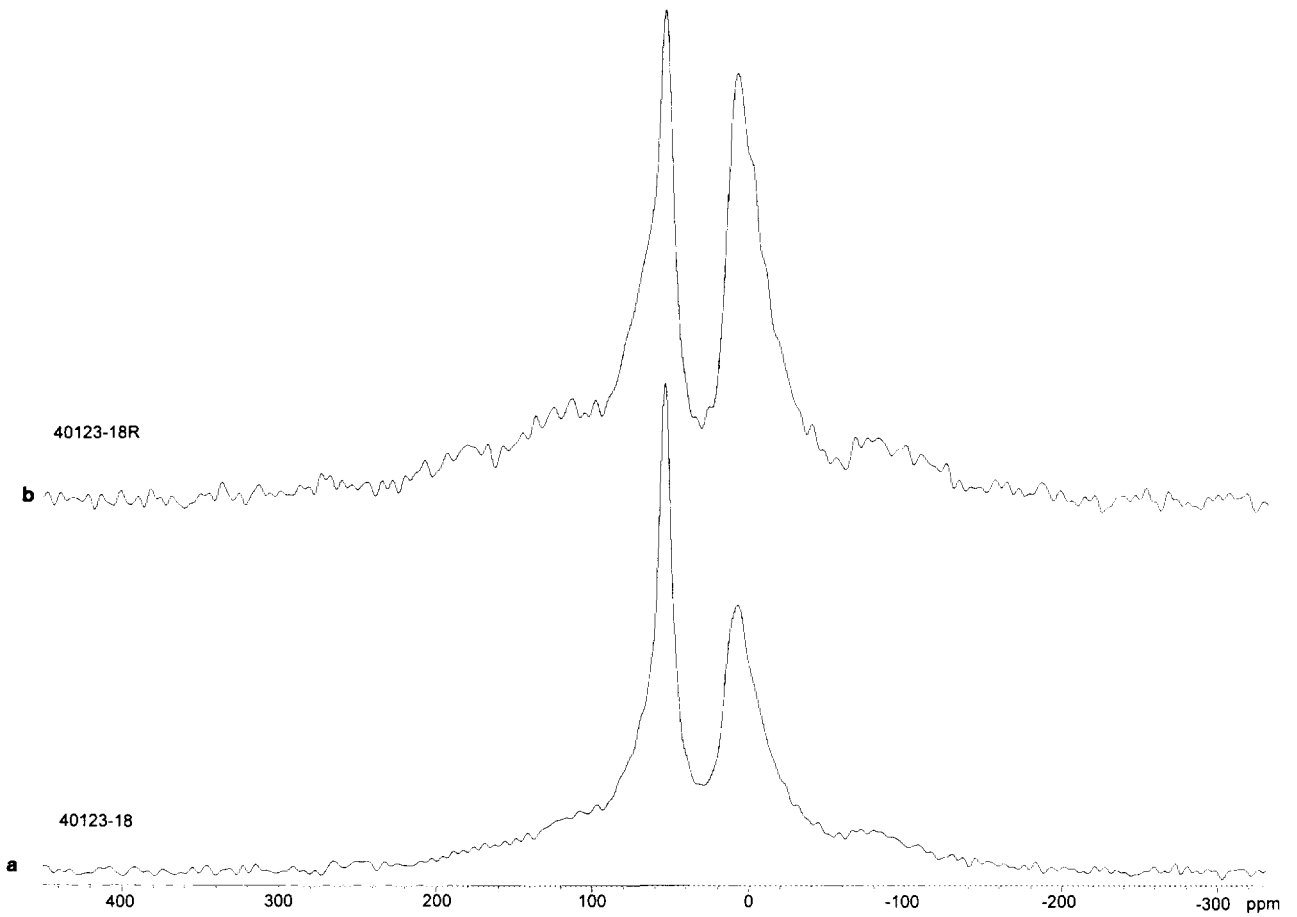

FIG. 3. ^{27}Al nonselective-echo MAS spectra of (a) fresh and (b) used ferrierite containing binder.

move large quadrupole aluminum sites from the spectrum as binder is present in these two catalyst samples.

The creation of nonframework aluminum after extended use could account for the reduction in catalyst selectivity in two ways. First, nonframework aluminum, if deposited in the zeolite channels would make egress of primary products more difficult, increasing the chances for secondary, nonselective reactions. Alternatively, nonframework alumina might be itself catalytically active but not particularly selective for butene isomerization. In either case dealumination upon use would result in reduced selectivity and in either case acid washing would be expected to remove the nonframework aluminum and restore selectivity.

Isothermal gravimetric adsorption studies using *n*-pentane as an adsorbate indicate no loss in adsorption capacity following extensive use. The fresh catalyst adsorbs about 5.5 wt% *n*-pentane based on catalyst zeolite content. On the same basis the used catalyst adsorbs 5.7% *n*-pentane. Adsorption studies do not suggest pore blockage following use. Tentatively, it might be concluded that the nonframework aluminum produced during regeneration contributes significantly to the production of non-C_4 products and that acid washing removes this aluminum and restores selectivity.

In summary, it is possible to achieve high selectivity and yields of isobutene with unmodified ferrierite but initial selectivity, prior to partial coke deactivation, is not high. In addition, degradive change occurs following extended use, rendering selectivity even lower.

Characterization of modified ferrierites. In an effort to reduce the high initial activity observed with unmodified ferrierite as well as to better understand changes that occur in ferrierite under hydrothermal conditions, a sample of unbound, hydrogen ferrierite powder, H–FER-2, was steamed at 873°K in a 100% steam atmosphere and designated S-FER-2. This steam treatment should simulate the effect of many cycles of use/regeneration. (In the pilot plant study, typical regeneration temperatures were kept below 813°K and steam partial pressures were calculated to be below 1%.) A portion of this steamed sample was given a subsequent hydrochloric acid-wash treatment and designated SAW-FER-2. Finally, a portion of this steamed–acid-washed ferrierite was given an additional steam treatment and designated SAWS-FER-2. The S-FER-2 and SAW-FER-2 samples were extensively characterized; all samples were also alumina bound and evaluated at the bench scale for butene isomerization performance.

Results of X-ray diffraction studies are summarized in Table 1. Unit cell parameters and cell volumes are presented for fresh, steamed, and steamed–acid-washed ferrierite. In addition, relative crystallinities are presented using the fresh ferrierite, H-FER-2, as a basis for comparison. It can be seen that the steam treatment causes a significant contraction in the *b*-axis of the unit cell, a lesser contraction in the *a*-axis, and has almost no effect on the *c*-axis. No loss of crystallinity was observed. Results are consistent with a steam-induced partial dealumination of the zeolite crystal. Subsequent acid washing produces no significant effect in the unit cell parameters.

TABLE 1

X-Ray Diffraction Analysis: Unit Cell Parameters and Relative Crystallinity

Samples	Unit cell parameters (Å)			Cell volume	Normalized integrated peak areas
	a	*b*	*c*		
H-FER-2	18.897	14.161	7.4489	1993	100%
S-FER-2	18.862	14.081	7.4489	1978	105%
SAW-FER-2	18.869	14.084	7.4498	1980	119%

Zeolite dealumination upon steaming is also evidenced by the diffuse reflectance infrared analysis presented in Table 2 for the same three samples. Bands at 1066 and 780 cm^{-1}, associated with asymmetric and symmetric stretching of H-FER-2 T–O groups, respectively, are found to shift upon steam treatment. Results are consistent with those reported in the literature (13) and attributed to framework dealumination. As with XRD analysis, infrared data suggest that subsequent acid washing causes no additional framework dealumination.

The extent of framework dealumination caused by steaming is suggested by aluminum MAS-NMR spectra plotted in absolute intensity for the three samples in Fig. 4. In this figure ^{27}Al short pulse MAS-NMR spectra are presented for (a) unmodified ferrierite, H-FER-2, (b) steamed ferrierite, S-FER-2, and (c) steamed–acid-washed ferrierite, SAW-FER-2. Note that with the unbound H-FER-2 powder, there is only a small resonance due to octahedral aluminum at 0 ppm. Most aluminum is in the tetrahedral form in the fresh sample. The tetrahedral aluminum resonance at 58 ppm observed with the fresh sample is greatly reduced for both the steamed and the steamed–acid-washed samples, consistent with framework dealumination. A slight increase in the octahedral resonance is observed but does not correspond to the decreased intensity of tetrahedral aluminum. The signal to noise is lower

TABLE 2

IR Band Frequencies of T–O Stretching Modes (in cm^{-1})

Sample	ν Asymmetric T–O	ν Symmetric T–O
H-FER-2	1066	780
S-FER-2	1083	820
SAW-FER-2	1082	819

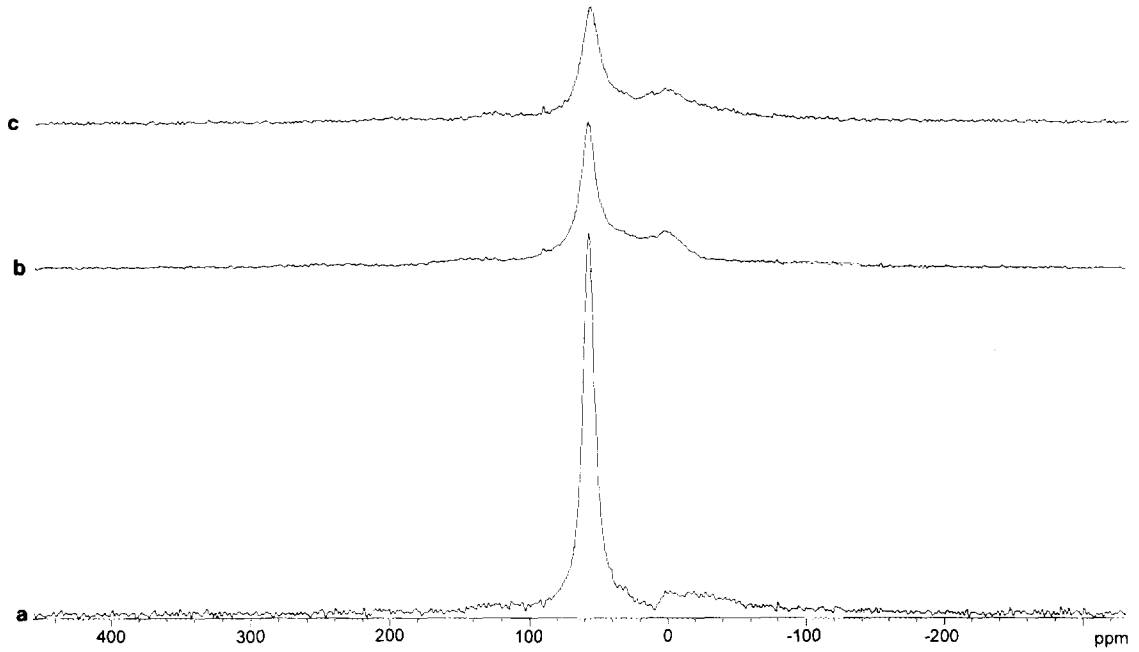

FIG. 4. ^{27}Al short pulse MAS-NMR spectra of (a) unmodified ferrierite, H-FER-2, (b) steamed ferrierite, S-FER-2, and (c) steamed–acid-washed ferrierite, SAW-FER-2.

on the fresh ferrierite sample because it was accumulated for only $\frac{1}{8}$ of the number of pulses under the same conditions as the two treated ferrierites. The figure demonstrates the loss of aluminum from the ferrierite framework and the increased asymmetry of the extraframework aluminum formed in the dealuminated samples. This increasing asymmetry is shown by the loss of the signal from certain asymmetric extra-framework sites, owing to their short T_2's, and subsequent nonobservation, owing to the 10-μs dead time before acquisition of the signal in the short pulse-and-acquire sequence.

While XRD, IR, and Al-MAS-NMR suggest significant changes following steam treatment, zeolite compositional changes are small. Silicon/aluminum atom ratios as determined by chemical and X-ray photoelectron spectroscopy (XPS) analysis are summarized in Table 3. Data are presented for fresh, steamed, and steamed–acid-washed samples. As expected, steam treatment does not change the overall silicon/aluminum ratio as determined by chemical analysis. The steamed–acid-washed ferrierite shows that only minor dealumination has occurred following the acid-wash step. This agrees with literature reports on steamed–acid-washed ferrierite (13) and contrasts sharply with effects observed in other zeolites such as faujasite where steam–acid-wash treatment was used to achieve high dealumination (23, 24). Apparently the nonframework aluminum formed by steam treatment of ferrierite is only partially soluble in aqueous acid solution. According to X-ray photoelectron spectroscopy, which provides surface chemical analysis, both modified ferrierites are partially silicon-enriched by treatment. The increase in surface silicon upon steaming is unexpected; literature studies with Y zeolite (25) indicate that steam treatment causes aluminum deposition on the zeolite surface, resulting in a decreased silicon/aluminum ratio. Apparently with ferrierite, the nonframework aluminum created by steam treatment does not migrate to the zeolite surface. This fact plus the inability of acid treatment to significantly lower zeolite aluminum content suggests that nonframework aluminum may be trapped within the zeolite crystal.

TABLE 3

Silicon/Aluminum Ratios as Determined by Chemical Analysis and by X-Ray Photo-Electron Spectroscopy (XPS)

	Silicon/aluminum ratios by	
Sample	Chemical analysis	XPS
H-FER-2	8.9	8.8
S-FER-2	8.9	11.1
SAW-FER-2	9.2	11.8

Adsorption capacities for the fresh and treated samples were gravimetrically determined using n-pentane and carbon dioxide as adsorbates at a P/P_0 of 0.1. n-Pentane with an estimated kinetic diameter of 4.3 Å (26) should access ferrierite's 10-MR channels (5.4 × 4.2 Å) but be excluded

from its 8-MR channels (3.5 × 4.8 Å), whereas carbon dioxide with a kinetic diameter of 3.3 Å should access both channel systems. Results are reported on a volumetric basis in Table 4, assuming liquid densities for adsorbates. The data show increased *n*-pentane capacity upon steaming; this is consistent with results obtained with the used ferrierite catalyst sample, used-FER-1. A further increase is observed upon acid treatment. Using carbon dioxide as an adsorbent, uptake is similar to that observed with pentane for both the fresh and steamed ferrierites. Constant pressure sorption modeling of *n*-pentane and carbon dioxide at experimental temperature and partial pressures were conducted to calculate ideal loading and help interpret the experimental results. *n*-Pentane was adsorbed in the 10-MR channels and the calculated adsorption capacity is similar to experiment. Carbon dioxide was adsorbed in the 8-MR channels as well as the 10-MR channels. The calculated results are considerably larger than the experimental results and imply that in actuality, CO_2 does not have clear access to the 8-MR channel. Based on the similar experimental results obtained with the two adsorbates, it appears that carbon dioxide does not access ferrierite's 8-MR channel system and so adsorption studies cannot determine the state of the smaller channels following steam treatment. However, based on the increased capacity of S-FER-2 for both *n*-pentane and carbon dioxide, it does not appear that nonframework aluminum created by steam treatment is located in ferrierite's 10-MR channels.

There are two potential locations for the nonframework aluminum species within steamed ferrierite that are consistent with the characterization described above. First, aluminum species might be located in the 8-MR channels. This possibility is supported by modeling studies, conducted to determine preferred sites and mobility of aluminum species within the ferrierite crystal. Constant loading sorption modeling was conducted at 873°K to mimic steaming conditions and as a first guess Al(OH)3 and Al(O)OH were selected as likely products of framework dealumination. Results for Al(O)OH sorbate modeling are graphically displayed in Fig. 5, which shows the energetically preferred positions by plotting the Al(O)OH center of mass as points in the ferrierite framework. Model sorption studies show that Al(O)OH and Al(OH)3 can be located throughout the length of 10-MR ring channel but can only occupy isolated locations in the 8-MR channel at the intersections of the 6- and 8-MR channels. Energy minimization at low loading shows that siting in the 6–8 intersection is about the same energetically as siting in the 10-MR channel. If aluminum species formed at the intersection of the 6- and 8-MR channels during steam treatment, they would be as stable as in the 10-MR channel; however, because of energy barriers they could not move away from this location. These modeling results are consistent with our observations that aluminum debris does not block the 10-MR channel and is very difficult to remove by subsequent acid-wash treatment.

TABLE 4

Gravimetric Adsorption Capacities for Ferrierite and Modified Ferrierites at $P/P_0 = 0.1$

Sample	Adsorbate (wt%)		Adsorbate (cc/100g)[a]	
	n-Pentane	Carbon dioxide	*n*-Pentane	Carbon dioxide
H-FER-2	5.7%	11.5%	9.1	10.4
S-FER-2	6.7%	10.5%	10.7	9.5
SAW-FER-2	7.1%	11.2%	11.3	10.2
Model prediction	5.0%	15.4%	8.0	14.0

[a] Assuming an *n*-pentane density of 0.626 cc/g and a carbon dioxide density of 1.105 cc/g.

However, there is also a second possible location for framework aluminum. Conceivably it might be located at the site of defects or voids within the zeolite crystal created by steam treatment. The presence of these voids in steamed Y zeolite is well documented (27–29). These mesoporous cavities form as a result of the coalescence of individual vacancies created by the loss of alumina tetrahedra under steaming conditions. The coalescence is driven by a reduction in surface tension as microvoids combine. Transmission electron microscopy of thin sections of steamed ferrierite, S-FER-2, are presented in Fig. 6. Ferrierite is composed of micrometer-sized platelets, about 0.2–0.3 μm in thickness. TEM of ferrierite provides views from either the edge or face of these platelets. The presence of voids or mesopores within the steamed crystal is apparent both in Fig. 6a, a face view, and in Fig. 6b, an edge-on view. Voids range in size from 20 to 200 Å. Obviously, aluminum debris deposited in these voids would not block adsorption in the crystal channel system. Furthermore, the creation of these voids upon hydrothermal treatment may explain the improved adsorption capacity observed with S-FER-2 and the used-FER-1 samples. It is interesting to note that the voids created by steaming ferrierite appear to be structured. When viewed from the face of a ferrierite crystal platelet (as in Fig. 6a), voids present a rectangular to square appearance but when viewed from the edge of a sectioned platelet, voids appear elongated and slit-like (as in Fig. 6b). This contrasts with the nonstructured, spherical voids observed in steamed faujasite samples. The structured voids suggest that with ferrierite there are crystal planes with enhanced lability under hydrothermal conditions.

Performance of modified ferrierite catalysts. The fresh and modified ferrierite powders were alumina bound and formed for catalytic testing at the bench scale with 1-butene feed. The conditions of the test were the same as described

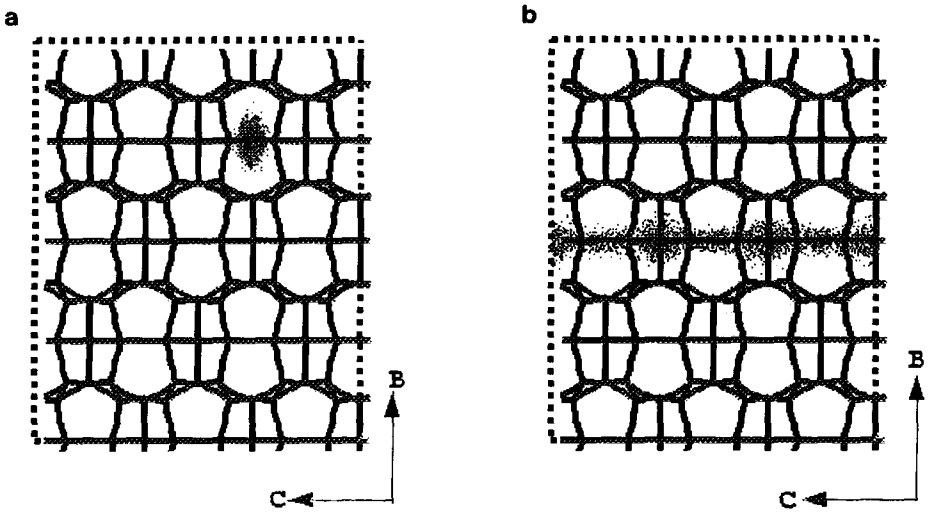

FIG. 5. Possible center-of-mass distributions for Al(O)OH species in (a) 8-MR channel and in (b) 10-MR channel of ferrierite as calculated by molecular modeling experiments.

above. Total linear butene conversions are plotted as a function of time on feed in Fig. 7. Data are presented for the fresh H-FER-2 as well as for the steamed (S-FER-2) and the steamed–acid-washed (SAW-FER-2) ferrierites. As seen before, the fresh, unmodified ferrierite has high activity for butene conversion. This initial hot activity is lost as the catalyst undergoes coke deactivation. Steaming very significantly reduces initial conversion relative to the fresh catalyst. The steamed–acid-washed ferrierite also exhibits reduced initial activity. Both the steamed and the steamed–acid-washed samples exhibit a reduced deactivation rate relative to the unmodified ferrierite so that after several hours on feed the fresh and modified catalyst all exhibit similar *n*-butene conversions.

It is not readily apparent from Fig. 7 how catalyst selectivity is affected by the modifications described. In order to evaluate selectivities it is best to compare catalyst yields at equivalent conversion levels and with comparable coke deposition since catalyst coking may be expected to alter selectivity. The effect of coke deposition on the selectivity of modified ferrierites will be described in a future publication. For the present study product yields were obtained at varying conversion levels as the catalysts underwent deactivation by coking. The product yields obtained in this fashion are compared in Fig. 8 where yields of isobutene and non-C_4 products are plotted against conversion. Data are provided for H-FER-2, S-FER-2, SAW-FER-2, and SAWS-FER-2. From the figure it can be seen that steaming significantly decreases isobutene yields relative to unmodified ferrierite when both are compared at equal conversion. Decreased isobutene selectivity is accompanied by an increased production of non-C_4 products relative to the fresh catalyst. It should be recalled that a similar but even larger effect was observed following extended use/regeneration in the pilot plant evaluation. Acid-wash treatment of the steamed ferrierite greatly enhances isobutene yield to a level slightly greater than that achieved with the unmodified ferrierite. Simultaneously, the steam–acid-wash treatment lowers non-C_4 product yields to a point slightly lower than that obtained with unmodified ferrierite. With SAW-FER-2, reduced initial activity (Fig. 7) with improved isobutene selectivity (Fig. 8) result in excellent start-of-run isobutene yields, as can be seen in Fig. 9 where isobutene yields for all samples are plotted as a function of time.

Based on the data in Fig. 7, it may be concluded that steaming removes some of the catalytic sites involved in butene conversion. However, from Fig. 8 the catalytically active sites remaining show an increased tendency to form non-C_4 products relative to the fresh catalyst. NMR, X-ray diffraction, and infrared characterization all indicate a significant framework dealumination following steam treatment. Together the results suggest that nonframework alumina created by steam treatment may be less active than framework aluminum for butene conversion but that this nonframework alumina is also significantly less selective for isobutene, catalyzing the production of non-C_4 products.

Also from Fig. 8 it is apparent that acid treatment of the steamed ferrierite improves selectivity for isobutene while reducing selectivity for non-C_4 products. NMR, X-ray diffraction, and infrared characterization all indicate that acid washing has no detectable effect on framework composition. However, chemical and XPS analysis do show a small but reproducible aluminum removal by acid treatment. It thus appears likely that acid washing partially removes some of the nonframework alumina formed dur-

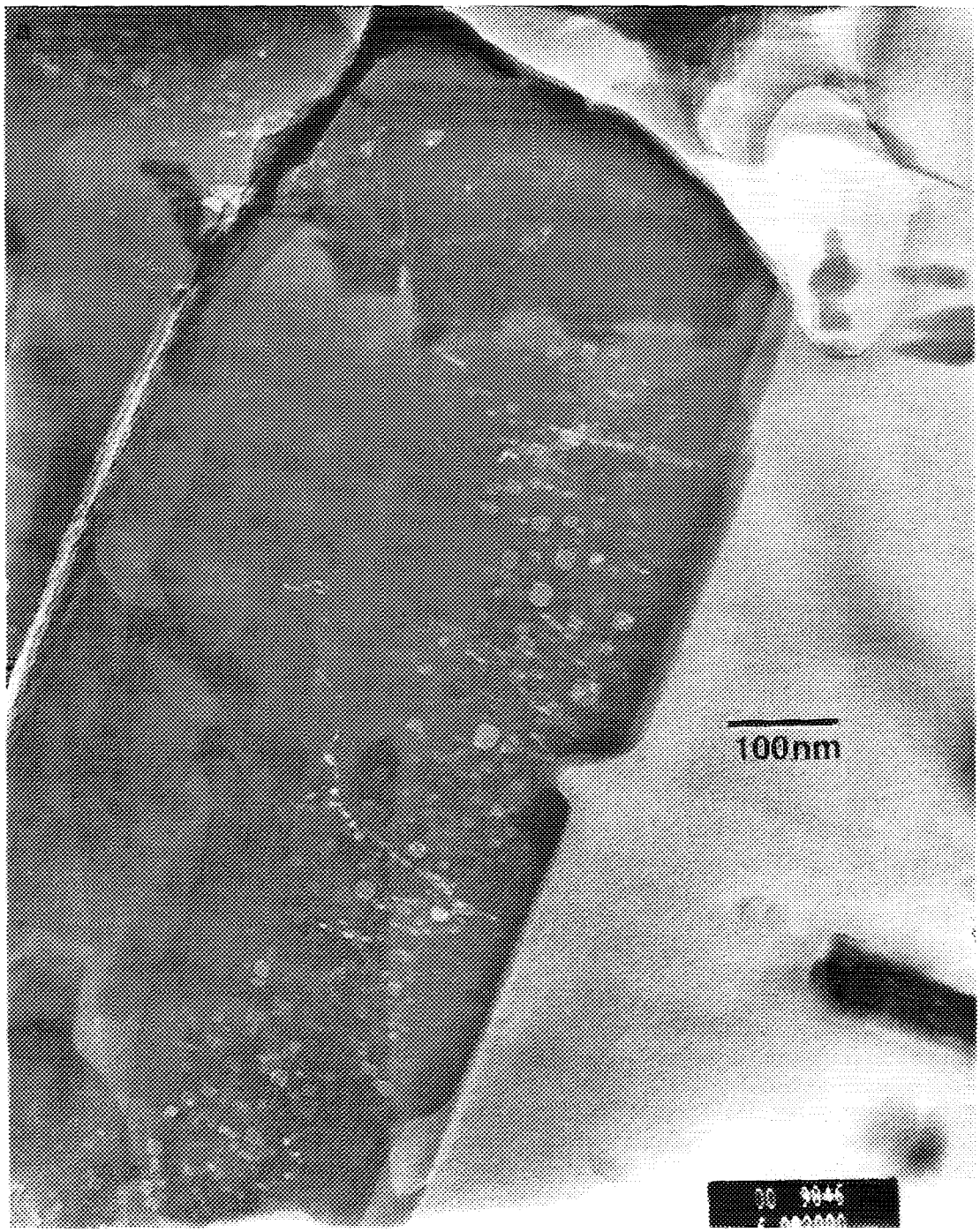

FIG. 6. Transmission electron micrograph of S-FER-2, showing the presence of mesoporous voids in the ferrierite crystal structure created by steaming as viewed from (a) the face and (b) the edge of ferrierite platelets.

ing steaming. The improved selectivity observed following acid washing is consistent with elimination of nonselective catalytic activity associated with the nonframework alumina created by steam treatment.

It can also be hypothesized that the catalytically active, nonframework aluminum is most likely deposited in the intracrystalline mesopores described above. Increased space within these voids permits the nonselective reactions observed. Aluminum in these voids is easily removed by acid treatment, resulting in improved selectivity. Apparently, most nonframework aluminum, not removed by acid washing, is deposited in the 8-MR channels; this alumi-

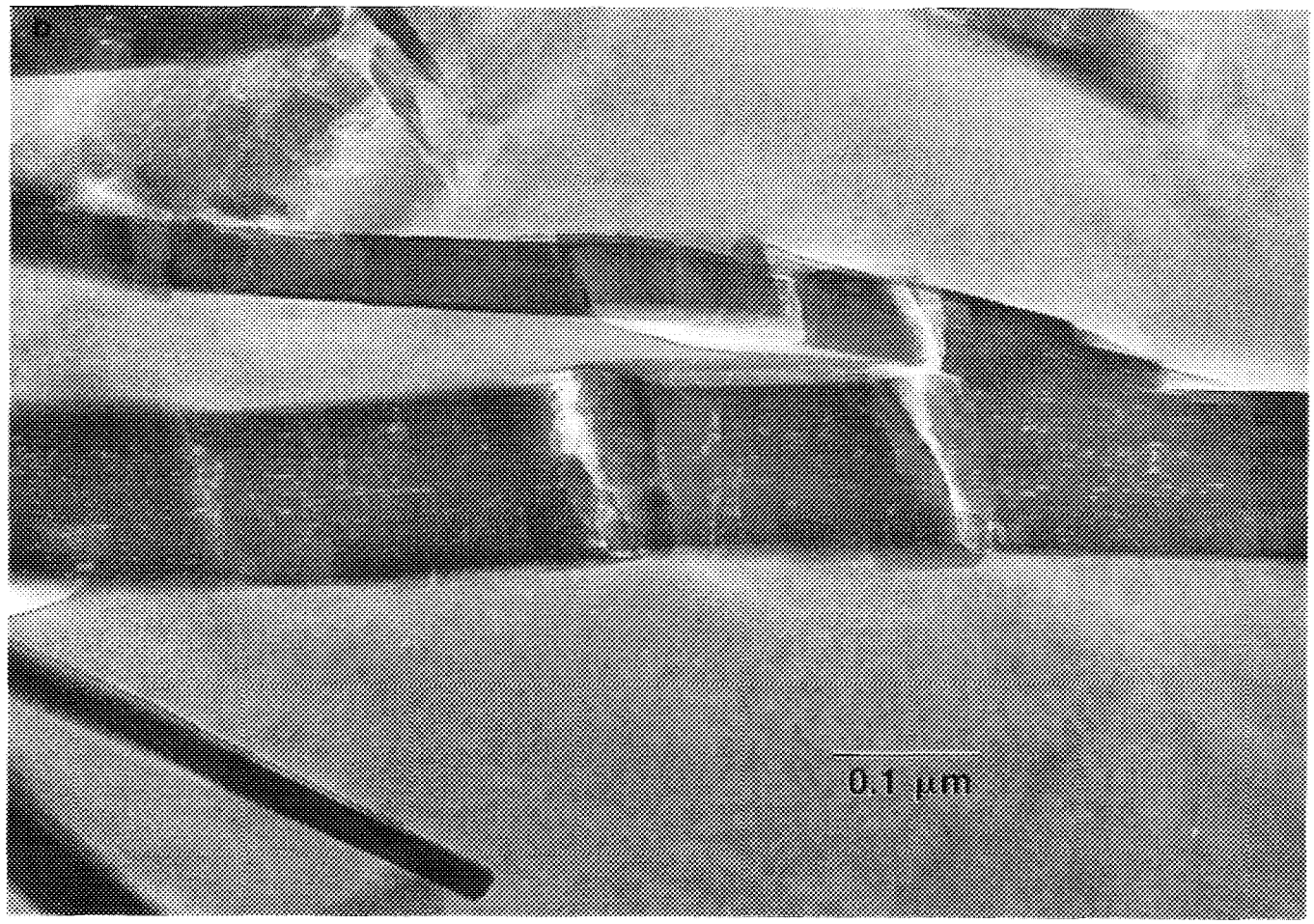

FIG. 6—*Continued*

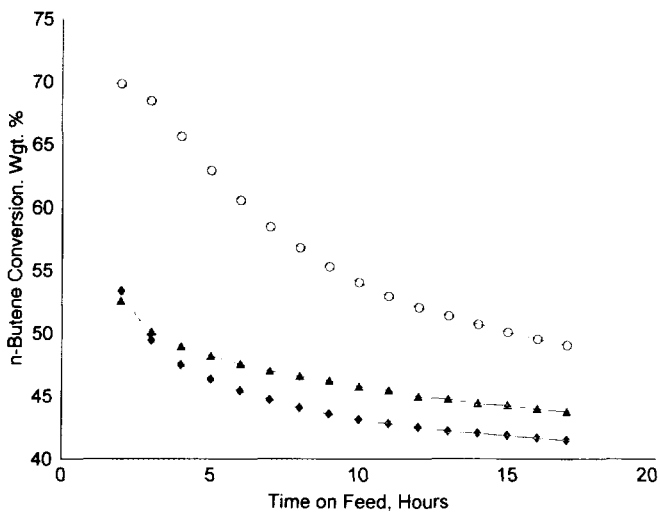

FIG. 7. Total *n*-butene conversion catalyzed by unmodified ferrierite, H-FER-2 (circles), steamed ferrierite, S-FER-2 (diamonds), and steamed–acid-washed ferrierite, SAW-FER-2 (triangles).

num is inaccessible and does not contribute to catalytic activity.

While steam–acid-wash treatment has important implications for the start-of-run performance, it should also have a very beneficial effect on long-term catalyst life (i.e., regenerability). This is suggested by the performance of SAWS-FER-2, shown in Figs. 8 and 9. The second steam treatment, applied to the already steamed–acid-washed ferrierite has little effect on selectivity. At comparable conversion levels, the SAWS ferrierite exhibits isobutene yields equivalent to those of the SAW and fresh ferrierites. Non-C_4 product yields remain relatively low. As already suggested by the catalyst characterization, the alumina debris formed by steaming is only partially removed by the acid-wash treatment. Framework aluminum remaining after steaming is not affected by acid washing. Thus both the remaining framework aluminum as well as the non-framework alumina must be relatively inert. That subsequent steam treatment has little effect on performance is consistent with a nonlabile, inert alumina phase, probably trapped in the 8-MR channels.

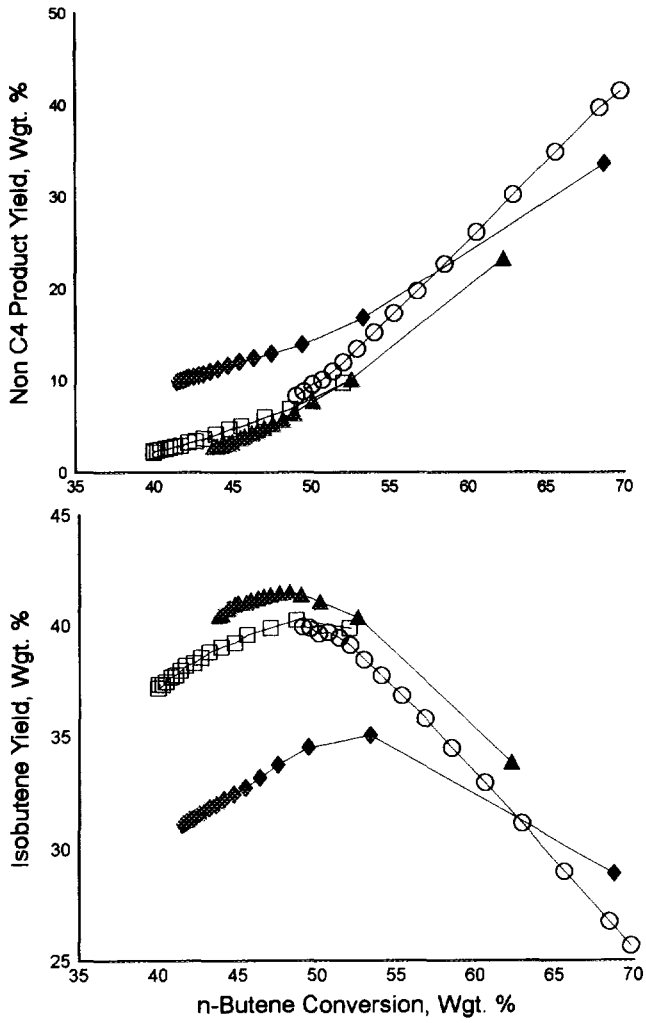

FIG. 8. Isobutene and non-C_4 product yields at varying conversion levels obtained with unmodified ferrierite, H-FER-2 (circles), steamed ferrierite, S-FER-2 (diamonds), steamed–acid-washed ferrierite, SAW-FER-2 (triangles), and steamed–acid-washed–steamed ferrierite, SAWS-FER-2 (boxes).

As a consequence, SAW ferrierite should not only have good start-of-run performance but should be much less sensitive to hydrothermal degradation caused by multiple regenerations. In an effort to assess longer term trends, SAW-FER-2 was evaluated for butene isomerization over 26 deactivation/regenerations cycles in the pilot reactor under a set of conditions very similar to those used in the pilot plant evaluation of FER-1. Following a final oxidative regeneration, a portion of this used catalyst, designated used-SAW-FER-2, was recovered, analyzed to contain less than 0.4% carbon, and then evaluated at the bench scale as described above. Results of these evaluations are presented in Fig. 10. Here product yields are plotted against linear butene conversions in order to allow comparisons

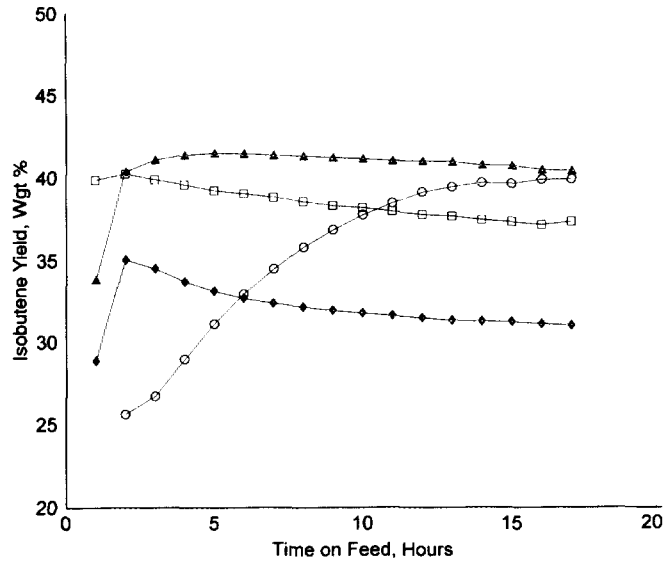

FIG. 9. Isobutene yields near the start-of-run: unmodified ferrierite, H-FER-2 (circles), steamed ferrierite, S-FER-2 (diamonds), steamed–acid-washed ferrierite, SAW-FER-2 (triangles), and steamed–acid-washed–steamed ferrierite, SAWS-FER-2 (boxes).

to be made between catalysts at similar conversion levels. Data obtained with used-FER-1, described earlier, are also presented for comparison. From Fig. 10, there is a small decrease in conversion (i.e., activity) for used-SAW-FER-2 compared to the fresh SAW-FER-2; however, the yield of isobutene at comparable conversion remains almost unaffected by the 26 cycles of use and regeneration in the pilot plant. For example, at 45% conversion, fresh SAW-FER-2 yields 42% isobutene (93% isobutene selectivity) while

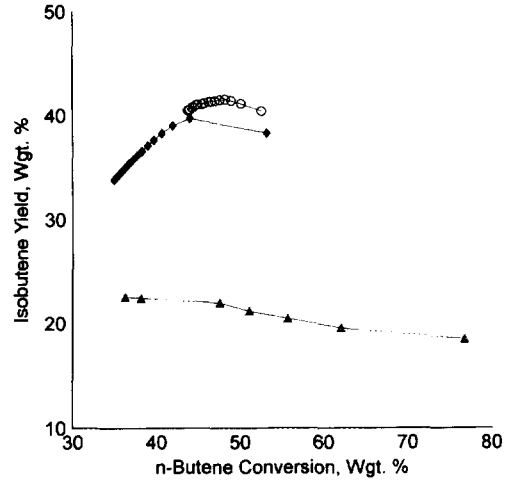

FIG. 10. Catalyst isobutene selectivity before extended use (SAW-FER-2, circles) and after extended pilot plant evaluation (used-SAW-FER-2, diamonds) and (used-FER-1, triangles).

used-SAW-FER-2 yields 40% isobutene (89% isobutene selectivity). By comparison and as noted earlier, used-FER-1 shows a drastic loss in isobutene yield after similar extended treatment, producing only 23% isobutene at the 45% conversion level (51% isobutene selectivity). The dramatic improvement in long-term stability of steamed–acid-washed ferrierite is attributed to the removal of labile alumina present in untreated H–FER-1. The aluminum remaining, both framework and nonframework, following SAW treatment is much less likely to migrate during use to cause a decrease in performance.

CONCLUSIONS

Fresh, unmodified ferrierite possesses active sites in excess of those required for isomerization of butenes to equilibrium (under the conditions of the present study). The excess activity is observed as additional butene conversion to non-C_4 products and reduced selectivity to isobutene. Deactivation by coke deposition reduces this initially high activity, resulting in an increase in isobutene yield with time on feed. The deactivation effect could be due to blocking of sites by carbon deposition or to spatial restrictions caused by carbon sterically limiting the nonselective reactions. Unmodified ferrierite's decrease in activity and isobutene selectivity following multiple run/regeneration cycles is accompanied by a loss of active framework sites and the creation of an amorphous aluminum phase, as indicated by aluminum MAS-NMR results.

Characterization of steamed as well as steamed–acid-washed ferrierites provides insight into changes occurring during extended use. Steam treatment eliminates some of the active sites responsible for the high initial *n*-butene conversion but creates other nonframework alumina sites which catalyze oligomerization and cracking. Subsequent acid washing of steamed ferrierite greatly reduces nonselective reactions by removing a fraction of this amorphous phase.

The characterization and performance data are consistent with the creation of two types of nonframework alumina. One type is located in the 8-MR channels, is relatively inert, and is resistant to extraction by acid treatment. The second type is located in mesoporous voids created by steam. This type of alumina is catalytically active but nonselective for isomerization. Fortunately, this type of alumina is easily removed by acid washing.

The steamed–acid-washed ferrierite exhibits greatly reduced sensitivity to subsequent steam treatment in comparison to unmodified ferrierite. This improved hydrothermal stabiliy is attributed to the removal of the labile aluminum sites present in unmodified ferrierite.

ACKNOWLEDGMENTS

The authors thank Texaco Development Corp. for permission to publish this work. In addition, the authors thank J. Edwards for MAS-NMR analysis, P. Cusatis and C. Y. Thiel for diffuse reflectance FTIR, R. Pugliese for X-ray diffraction results and interpretation, and P. L. Dahlstrom for X-ray photoelectron spectroscopy.

REFERENCES

1. Unzelman, G. H., *Fuel Reformulation* **2**(3), 16 (1992).
2. Butter, A. C., and Nicolaides, C. P., *Catal. Today* **18,** 443 (1993).
3. Grandvallet, P., deJong, K. P., Mooiweer, H. H., Kortbeek, A. G. T., and Karushaar-Czarnetzki, B., European Patent 501,577, 1992.
4. Powers, D. H., Murray, B. D., Winquist, B. H. C., Callender, E. M., and Varner, J. H., European Patent 523,838, 1992.
5. Barri, A. A. I., and Kidd, D. A., European Patent 485,145, 1991.
6. Thomas, J. M., *Sci. Am.*, Apr., 112 (1992).
7. Haggin, J., *Chem. Eng. News*, Oct., 25 (1993).
8. Xu, W.-Q., Yin, Y.-G., Suib, S. L., and O'Young, C.-L., *J. Catal.* **150,** 34 (1994).
9. Mooiweer, H. H., deJong, K. P., Kraushaar-Czarnetzki, B., Stork, W. H. J., and Krutzen, B. C. H., *in* "Zeolites and Related Microporous Materials: State of the Art 1994" (J. Weitkamp *et al.*, Eds.), p. 2327, Elsevier, Amsterdam/New York, 1994.
10. O'Young, C.-L., Pellet, R. J., Casey, D. G., Ugolini, J. R., and Sawicki, R. A., *J. Catal.* **151,** 467 (1995).
11. Vaughan, P. A., *Acta Crystallogr.* **21,** 983 (1966).
12. Xu, W.-Q., Yin, Y.-G., Suib, S. L., and O'Young, C.-L., *J. Phys. Chem.*, **99,** 758 (1995).
13. Jin, Y. S., Auroux, A., and Vedrine, J. C., *Appl. Catal.* **37,** 21 (1988).
14. Solomon, I., *Phys. Rev.* **110,** 61 (1958).
15. Warren, W. W., and Norberg, R. E., *Phys. Rev.* **154,** 277 (1967).
16. Man, P. P., Klinowski, J., Trokiner, A., Z. H., and Papon, P., *Chem. Phys. Lett.* **151,** 143 (1988).
17. Kibby, C. J., Perrolta, A., and Massoth, F. E., *J. Catal.* **35,** 256 (1974).
18. All modeling results were generated using the program Cerius. This program was developed by Molecular Simulations Inc.
19. Burchart, E. de Vos, Ph.D. Thesis, "Studies on Zeolites: Molecular Mechanics, Framework Stability, and Crystal Growth," Technische Universiteit Delft, 1992.
20. Rappé, A. K., Casewit, C. J., Colwell, K. S., Goddart, W. A., and Skiff, W. M., *J. Am. Chem. Soc.* **114,** 10,024 (1992).
21. Rappé, A. K., and Goddard, W. A., *J. Phys. Chem.* **95,** 3358 (1991).
22. The thermodynamic data for the four butene isomers were calculated by using changes of Gibbs free energy in Rossini, F. D., Pitzer, K. J., Arriett, R. L., Braum, R. M., and Pimentel, G. C., "Selected Values of Physical and Thermodynamic Properties of Hydrocarbons and Related Compounds," The American Petroleum Institute, Project 44, Carnegie Press, Pittsburgh, 1953.
23. Corma, A., Grande, M., and Fornes, V., *Appl. Catal.* **66,** 45 (1990).
24. Chevreau, T., Chambellan, A., Lavalley, J. C., Catherine, E., Marzon, M., Janin, A., Hemidy, J. F., and Khabtou, S., *Zeolites* **10,** 226 (1990).
25. Gross, T., Lohse, U., Engelhardt, G., Richter, K.-H., and Patzelova, V., *Zeolites* **4,** 25 (1984).
26. Breck, D. W., "Zeolite Molecular Sieves." Wiley, New York, 1974.
27. Patzelova, V., and Jaeger, N. I., *Zeolites* **7,** 240 (1987).
28. Pellet, R. J., Blackwell, C. S., and Rabo, J. A., *J. Catal.* **114,** 71 (1988).
29. Weber, G., and Simonot-Grange, M.-H., *Zeolites* **14,** 433 (1994).